Analytical and Bioanalytical Chemistry (2022) 414:6259–6269
https://doi.org/10.1007/s00216-022-04198-x

RESEARCH PAPER

Effect of ion source polarity and dopants on the detection of auxin plant hormones by ion mobility-mass spectrometry

Vahideh Ilbeigi[1] · Younes Valadbeigi[2] · Ladislav Moravsky[1] · Štefan Matejčík[1]

Received: 25 April 2022 / Revised: 20 June 2022 / Accepted: 23 June 2022 / Published online: 7 July 2022

Abstract

Ion mobility spectrometry (IMS) equipped with a corona discharge (CD) ion source was used for measurement of three auxin plant hormones including indole-3-acetic acid (IAA), indole-3-propionic acid (IPA), and indole-3-butyric acid (IBA). The measurements were performed in both positive and negative polarities of the CD ion source. Dopant gases NH_3, CCl_4, and $CHBr_3$ were used to modify the ionization mechanism. A time-of-flight mass spectrometer (TOFMS) orthogonal to the IMS cell was used for identification of the product ions. Density functional theory was used to rationalize formation of the ions, theoretically. The mixtures of the auxins were analyzed by CD-IMS. The separation performance depended on the ion polarity and the dopants. In the positive polarity without dopants, auxins were ionized via protonation and three distinguished peaks were observed. Application of NH_3 dopant resulted in two ionization channels, protonation, and NH_4^+ attachment leading to peak overlapping. In the negative polarity, two ionization reactions were operative, via deprotonation and O_2^- attachment. The separation of the monomer peaks was not achieved while the peaks of anionic dimers $[2\ M\text{-}H]^-$ were separated well. The best LOD (4 ng) was obtained in negative polarity with CCl_4 dopant. Methylation (esterification) of IAA improved LODs by about one order.

Keywords Plant hormone · Ion mobility spectrometry · Auxin mixture · Halide attachment

Introduction

Auxins are an important class of plant hormones or phytohormones with an aromatic ring and a carboxylic acid group [1]. Indole-3-acetic acid (IAA), indole-3-propionic acid (IPA), and indole-3-butyric acid (IBA) are the most important members of this class (Fig. 1).

These plant hormones are distributed in all parts of plants including root, leaves, flowers, and fruits with different concentrations [2]. Auxins are essential for plant growth, root initiation, seed dispersal, and fruit growth and development, and they control the shape of the plants and induce cell division and cell elongation [3–6]. Also, they play roles in flowering and it can delay the senescence of flowers [7]. Hence, different techniques and methods have been used for determination of auxins and their derivatives.

Chromatographic techniques are the most prevalent methods that have been used for determination of auxins and other plant hormones [8–11]. Because of the very low concentration of the plant hormones in plant tissues (0.1–50 ng g^{-1}) [9], the chromatographic techniques have been coupled with mass spectrometry (MS) to achieve higher sensitivity [12–19]. Since auxins have a polar COOH group, derivatization is used to increase their volatility in gas chromatography (GC) or decrease their hydrophilic property for measurements in liquid chromatography (LC) [12, 20–22]. In the case of LC and GC measurements with UV or fluorescence detectors, UV-absorbing and fluorescent groups are added to analyte during derivatization [23]. Capillary electrophoresis (CE) with

✉ Vahideh Ilbeigi
vahideh.ilbeigi@fmph.uniba.sk

✉ Štefan Matejčík
stefan.matejcik@fmph.uniba.sk

[1] Department of Experimental Physics, Faculty of Mathematics, Physics and Informatics, Comenius University in Bratislava, Mlynská dolina F2, 84248 Bratislava, Slovakia

[2] Department of Chemistry, Faculty of Science, Imam Khomeini International University, Qazvin, Iran

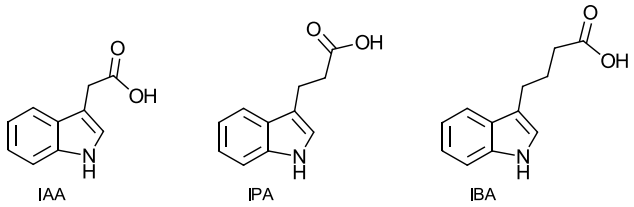

Fig. 1 Chemical structures of indole-3-acetic acid (IAA), indole-3-propionic acid (IPA), and indole-3-butyric acid (IBA)

electrochemiluminescent detection has been also used for measurement of auxins; however, this technique requires derivatization of auxin with some imides [24]. Over the last two decades, different types of biosensors (mainly fluorescence-based) have been developed for monitoring of plant hormones with subcellular resolution [25–27].

Ion mobility spectrometry (IMS) is a fast and sensitive technique for detection of ions in gas phase [28]. The produced ions move toward a detector under an electric field through a drift gas, N_2, or air mainly. Separation of different ions in the drift region is based on the difference in the collisional cross sections of the ions with the drift gas molecules [29]. Although a wide range of ionization sources have been used with IMS, electrospray ionization (ESI) and atmospheric pressure chemical ionization (APCI) are the prevalent ionization mechanisms in IMS [28]. These ion sources are able to work in both negative and positive modes.

In the positive APCI, ionization is mainly based on protonation or proton transfer from an initial ions called reactant ions (RIs) to the analyte and formation of $[M+H]^+$ ions [28, 30]. In the presence of higher concentration of the analyte, proton-bound dimers, $[MH^+M]$, can be also formed [31–33]. In the negative APCI, ionization can proceed via deprotonation, electron, and anion attachment [34]. Using some additives or dopant gases, new RIs can be produced in the negative and positive modes which consequently influence the ionization mechanism [35–38]. The molecular structure of the analyte and the ionization mechanism determine the efficiency of ionization or amount of ion formation, hence, different ionization pathways lead to different sensitivity.

In this work, an ion mobility-time-of-flight mass spectrometer (IMS-TOFMS) equipped with an APCI-corona discharge (CD) is used for detection and separation of three auxins IAA, IPA, and IBA. The effect of positive and negative polarities of the CD ion source and the effect of different dopants on the ionization mechanism, sensitivity, and peak separation are investigated. Supporting density functional theory calculations were carried out to evaluate the thermochemistry data of the studied molecules and elucidate the ionization mechanisms.

Experimental

Instrumentation

The IMS-TOFMS used in this work was equipped with a point to plane CD-APCI ionization source operating in both positive and negative modes. The IMS-TOFMS was a homemade instrument constructed at the Department of Experimental Physics of Comenius University in Slovakia. A detailed description of the instrument can be found elsewhere [39]. The IMS drift tube operated at sub-ambient pressure (700 mbar) and temperature of 110 ± 2 °C (temperature of the exited drift gas) with a Faraday cup as the IMS detector in the end of the drift tube providing a resolution of 50 for IMS measurements. The flow rate of the drift gas (zero air) was 700 mL min^{-1}. A voltage of 8 kV was applied to the whole cell of IMS (12.5 cm) to provide a drift field of 640 V cm^{-1}. The CD was supplied by potential difference of 3 kV between the needle and plane electrodes. The IMS tube was connected to the differential pumping system through a 100 µm pinhole, and a stream of dry air gas was used in the interface of IMS and MS to keep the vacuum chamber from neutral molecules and water. The pumping system includes three chambers: the pressure of the first chamber was reduced to 0.1 mbar using two rotary pump, and the pressures of the second and third chambers were 10^{-5} and 5×10^{-6} mbar, respectively, provided by turbo molecular pumps. The length of TOF–MS tube was 54.7 cm with internal pressure of 10^{-6} mbar. A multichannel plate (MCP) was used as a detector for TOF–MS.

Materials and method

IAA (analytical standard, 98%), IPA (99%), IBA (99%), ammonium carbonate (99.999%), tetrachloride carbon (99%), bromoform (analytical standard), and methanol (99.9%) were Sigma-Aldrich products. The stock solutions of the analytes were prepared in methanol. To measure solution samples, a high temperature injection port was designed and constructed. The optimum temperature of the injection as 180 °C was established (see Electronic Supplementary Materials, Figure S1). For each measurement, 1 µL of the sample was injected into the injection port and the vaporized sample was transported to the ionization region using a carrier gas (dried air) with flow rate of 50 mL min^{-1}.

To modify the ionization mechanisms, dopant gases including NH_3 (in the positive mode), CCl_4, and $CHBr_3$ (in the negative mode) were injected into the ionization region. The ammonium carbonate was used as NH_3 source.

Dried air with flow rate of 5 mL min^{-1} was used to transport the dopant gas from the headspaces of ammonium carbonate, tetrachloride carbon, and bromoform to the ionization region. Schematic diagram of the experimental setup is shown in Fig. 2.

The methylation (esterification) of IAA was carried out using the method reported in [40]. Methylated IAA (IAA-ester) was prepared by adding 4 mL HCl 1 M and 4 mL CH_3OH to a tube containing 1 mL IAA with concentration of 1000 mg L^{-1}. The tube was capped and put in a water bath with temperature of 70 °C. In different time intervals (2–80 min), 1 µL of the sample was injected to IMS to monitor the progress of methylation reaction. It was found that the maximum methylation is achieved after 5 min (see Electronic Supplementary Materials Figure S2).

Computational details

The structures of neutral molecules and the adduct ions were fully optimized using DFT-B3LYP functional in the gas phase. The calculations were performed using the basis set 6–311 + + G(d,p) including diffuse and polarization functions for both hydrogen and heavier atoms. Frequency calculations were carried out at 25 °C at the same level of theory to compute thermodynamic quantities including enthalpies (ΔH) and Gibbs free energies (ΔG) of ion formation in the gas phase. Gaussian 09 software was used for all calculations [41].

Results and discussion

Positive polarity

Figure 3a compares ion mobility spectra of IAA, IPA, and IBA in the positive polarity in absence of dopants (air born RI). Only one IM-peak is observed for each of the auxins at drift times of 5.50, 5.67, and 5.88 ms, respectively. The increase in the drift time corresponds with the number of CH_2 groups in the alkyl chain of the auxins (Fig. 1). The mass spectra in Fig. 3b show that in the positive polarity, hydronium ions, $H^+(H_2O)_{1-4}$, are the main RIs and the protonated auxins are $[IAA+H]^+$, $[IPA+H]^+$, and $[IBA+H]^+$ the product ions.

Auxins have both nitrogen and oxygen atoms as proton acceptor sites. The comparison of the relative energies of the isomers $[IAA+H]^+$ and $[IPA+H]^+$ in gas phase reveals that oxygen atom of the C = O group is the most favored site of protonation for IAA and IPA (see Electronic Supplementary Materials Figure S3). However, because of the small difference between the basicities of oxygen and nitrogen atoms (2.8 and 13.8 kJ mol^{-1} for IAA and IPA, respectively), the nitrogen atoms can also be protonated but with lower abundances. For IBA, the nitrogen and oxygen atoms show comparable basicities and both N- and O-protonated isomers (protomers) can be formed in the ion source. The calculated proton affinities (PA) and gas phase basicities (GB) in Table S1 (Electronic Supplementary Materials) show that IAA, IPA, and IBA have more basicity than H_2O indicating that proton transfer from H_3O^+ to the auxins is thermodynamically favored. However, Fig. 3b shows that the larger hydronium clusters, $H^+(H_2O)_{3,4}$, are the most abundant RIs and direct proton transfer from these larger hydronium clusters to the auxins is not thermodynamically favorable, hence, the ionization proceeds via hydronium attachment followed by dehydration [30, 36]:

$$A + H^+(H_2O)_n \rightarrow [A + H^+(H_2O)_n] \rightarrow [A + H^+(H_2O)_x] + (n - x)\, H_2O \quad (1)$$

The hydronium attachment step is an exothermic and thermodynamically possible reaction. For example, the calculated ΔH and ΔG for $H^+(H_2O)_3^+$ attachment to IAA are − 115.4 and − 76.8 kJ mol^{-1}, respectively. The collisions

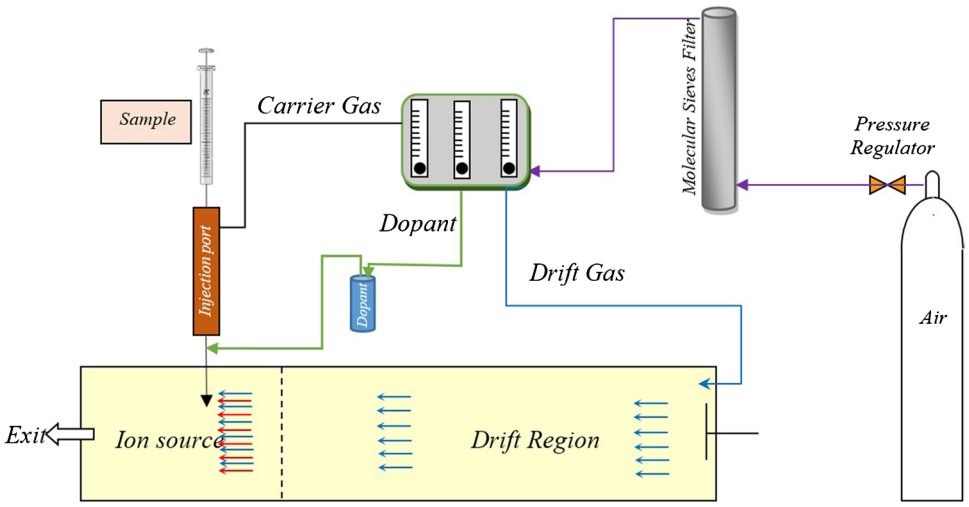

Fig. 2 Schematic representation of the experimental setup and the gas flow paths. The flow rates of drift, carrier, and dopant gases are 700, 50, and 5 mL $min.^{-1}$, respectively

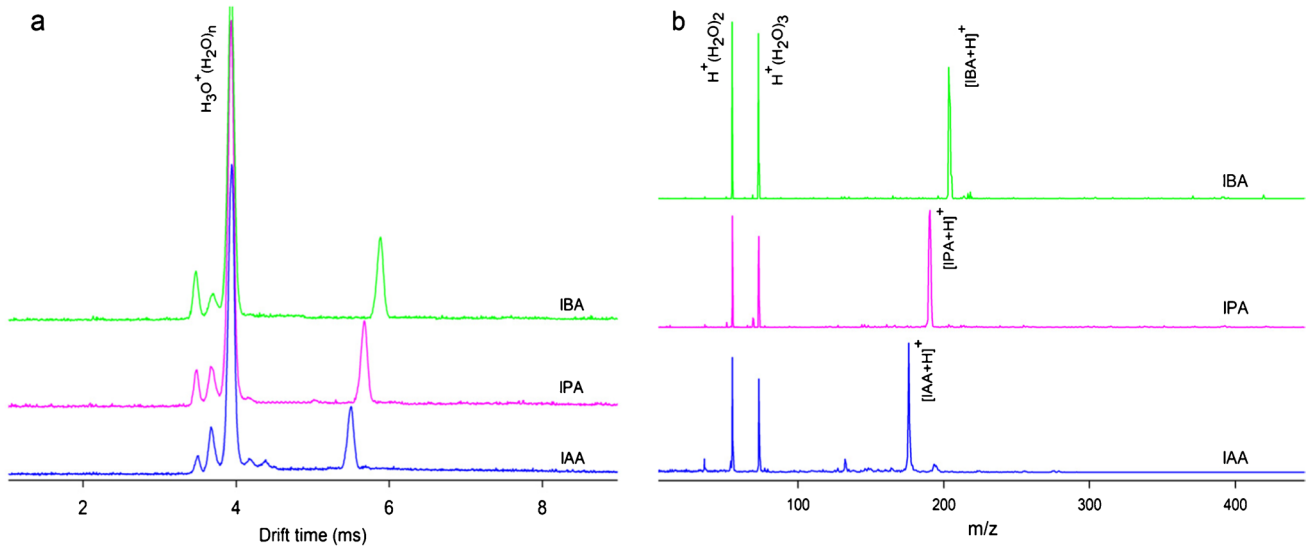

Fig. 3 Comparison of **a** ion mobility and **b** mass spectra of IAA, IPA, and IBA (30 mg $L.^{-1}$) in the positive mode of CD ion source

between drift gas molecules and $[IAA + H^+(H_2O)_n]$ provide the required energy for dehydration.

Figure 4a shows the IM-spectra of IAA, IPA, and IBA in the positive polarity in the presence of ammonium dopant. IAA shows only one IM-peak while two peaks were observed for IPA and IBA. The mass spectra in Fig. 4b show that IAA is ionized only by ammonium attachment while the ionization of IPA and IBA is carried out via both protonation and ammonium attachment reactions. Ammonium dopant replaces the air born RI by $NH_4^+(H_2O)_n$ RIs. The ionization mechanism of these RIs depends on the basicity of the analyte [36]. IAA with the calculated PA of ~ 850 kJ mol^{-1} is a weaker base than NH_3 (PA = ~ 854 kJ mol^{-1}) [42] and cannot capture the NH_4^+ proton (Table 1) while the ammonium attachment and formation of $[IAA + NH_4]^+$ is thermodynamically favored. IPA and IBA have higher basicities (PA = 868 and 865 kJ mol^{-1}, respectively) than NH_3. These isomers can be both protonated by NH_4^+, or form $[M + NH_4]^+$ clusters. Hence, two IM-peaks are observed for the IPA and IBA in the presence of NH_3 dopant. Optimized structures and relative energies of possible isomers of adduct cations of the auxins with NH_4^+ are shown in Figure S4 (Electronic Supplementary Materials). Comparison of

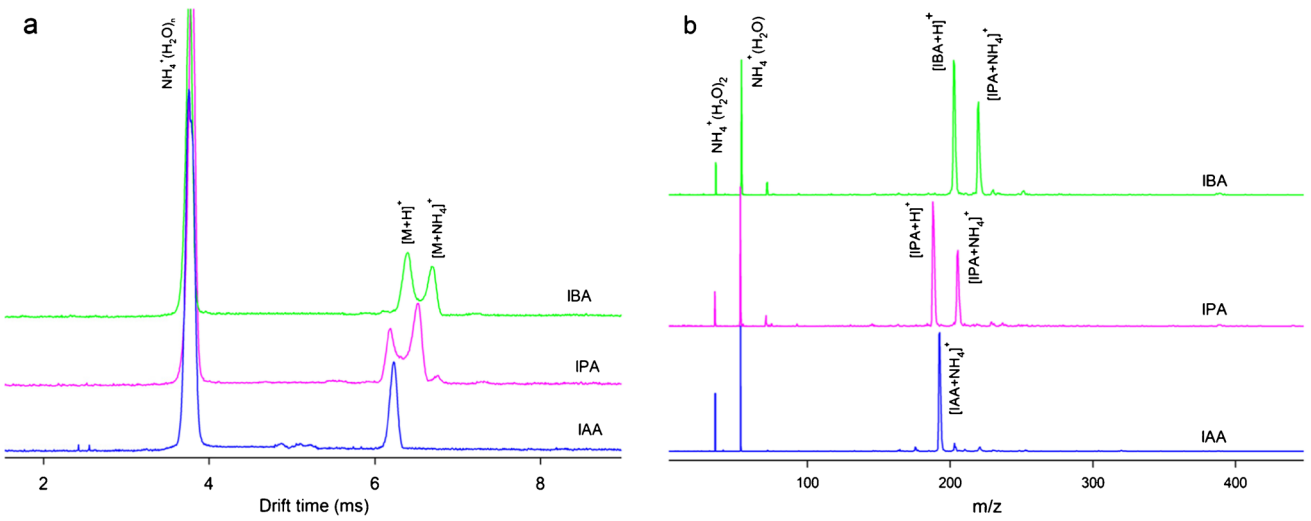

Fig. 4 Comparison of **a** ion mobility and **b** mass spectra of IAA, IPA, and IBA (30 mg $L.^{-1}$) in the positive mode of CD ion source with NH_3 as dopant

Table 1 The calculated ΔH and ΔG for protonation of the auxins by NH_4^+ and their NH_4^+ attachment. The energies are in kJ $mol.^{-1}$

Protonation	ΔH	ΔG	NH_4^+ attachment	ΔH	ΔG
$IAA+NH_4^+ \rightarrow [IAA+H]^+ + NH_3$	2.2	8.2	$IAA+NH_4^+ \rightarrow [IAA+NH_4]^+$	−150.5	−103.6
$IPA+NH_4^+ \rightarrow [IPA+H]^+ + NH_3$	−15.0	−3.9	$IPA+NH_4^+ \rightarrow [IPA+NH_4]^+$	−112.4	−78.5
$IBA+NH_4^+ \rightarrow [IBA+H]^+ + NH_3$	−12.2	−4.0	$IBA+NH_4^+ \rightarrow [IBA+NH_4]^+$	−151.5	−102.8

the relative energies shows that the C=O group is the most favored site for NH_4^+ attachment. However, the hydrogen bond C=O…HNH_3 is not the only interaction responsible for ammonium attachment and cation-π interaction causes a scorpion-like structure for the NH_4^+ adduct cations.

Negative polarity

Figure 5a displays the ion mobility spectra of IAA, IPA, and IBA in the negative polarity, in the absence of the dopants. Two main IM-peaks are observed for each auxin; however, for IAA, two additional small peaks are appeared in its IM-spectrum. The mass spectra show that the product ions responsible for these peaks are of different origin (Fig. 5b). The mass spectrum of IAA shows that the peaks at 5.5 and 7.8 ms are due to deprotonated monomer $[IAA\text{-}H]^-$ and dimer $[2IAA\text{-}H]^-$. The small ion mobility peak at 5.2 ms can be attributed to a fragment with m/z of 162 (Fig. 5b). This peak may be due to complexation of $[A\text{-}HCO_2]^-$ with O_2. Another small peak at 6.1 ms is probably due to adduct anion $[IAA+O_2]^-$ which is not observed in MS spectrum because of its dissociation after drift tube.

The mass spectra of IPA and IBA indicate that these compounds are ionized mainly via formation of the adduct anions with O_2^- rather than deprotonation. In other words, as the length of alkyl chain of auxins increases, their tendency for O_2^- attachment increases. Different ionization mechanisms of the auxins and resulting product ions are responsible for large difference in the drift times of ions formed from IAA and IPA.

The mass spectrum in Figure S5 (Electronic Supplementary Materials) shows that in the absence of dopants, $O_2^-(H_2O)_n$ and $CO_4^-(H_2O)_n$ are the reactant ions in negative mode which are responsible for the deprotonation and O_2-adduct formation of the auxins. A comparison of the relative stabilities of two isomers of CO_4^- reveals that this anion is in fact an adduct of CO_2 and O_2^-, $[CO_2+O_2]^-$, rather than a tetrahedral anion with carbon atom in the center (see Electronic Supplementary Materials Figure S6). The ΔH and ΔG for deprotonation of the auxins by O_2^- and $[CO_2+O_2]^-$ as well as formation of $[M+O_2]^-$ are summarized in Table 2. The comparison of the thermodynamic data shows that only O_2^- can deprotonate the auxins while the formation of adduct anions $[M+O_2]^-$ is possible in the presence of both O_2^- and $[CO_2+O_2]^-$. Interestingly, although predominantly CO_4^- is present in the ionization region, no $[M+CO_4]^-$ adduct ions were detected experimentally. This indicates that CO_4^- has most probably $[CO_2+O_2]^-$ form and it can produce the $[M+O_2]^-$ adduct followed by a CO_2 elimination. However, the data in Table 2 show that formation of

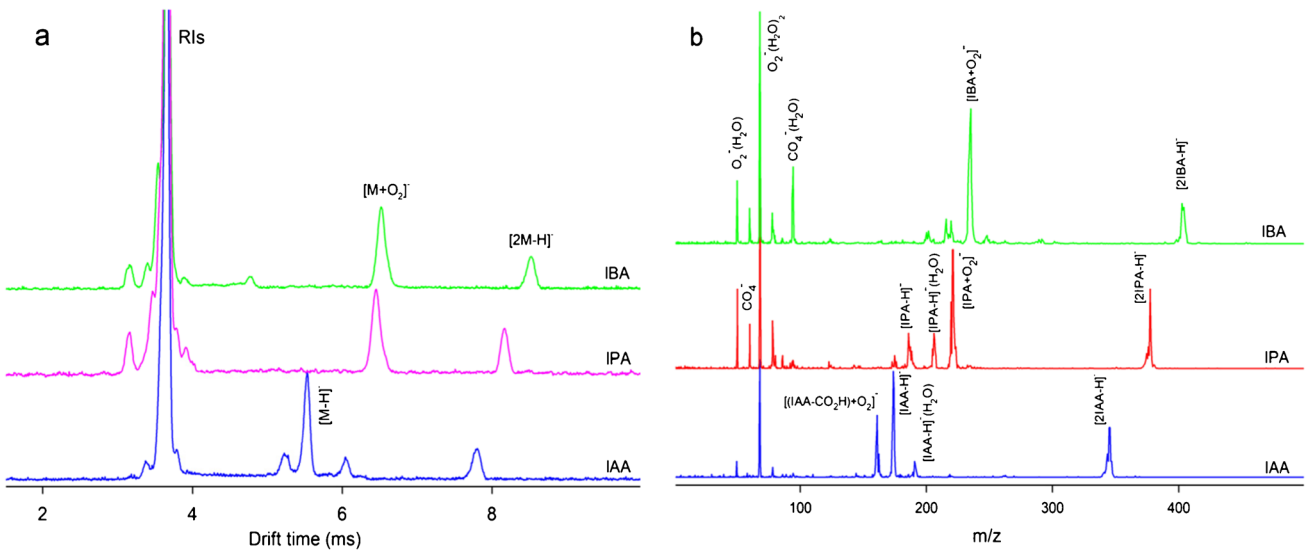

Fig. 5 Comparison of **a** ion mobility and **b** mass spectra of IAA, IPA, and IBA (30 mg $L.^{-1}$) in the negative mode of CD ion source

Table 2 The calculated ΔH and ΔG for deprotonation of the auxins by O_2^-, CO_4^-, Cl^-, and Br^- as well as anion attachments to the auxins in gas phase at 25 °C. The energies are in kJ $mol.^{-1}$

Deprotonation	ΔH	ΔG	Anion attachment	ΔH	ΔG
$IAA + O_2^- \rightarrow [IAA\text{-}H]^- + HO_2$	−42.1	−50.7	$IAA + O_2^- \rightarrow [IAA + O_2]^-$	−159.9	−130.5
$IPA + O_2^- \rightarrow [IPA\text{-}H]^- + HO_2$	−40.9	−44.2	$IPA + O_2^- \rightarrow [IPA + O_2]^-$	−165.2	−125.4
$IBA + O_2^- \rightarrow [IBA\text{-}H]^- + HO_2$	−40.5	−42.5	$IBA + O_2^- \rightarrow [IBA + O_2]^-$	−162.0	−121.6
$IAA + CO_4^- \rightarrow [IAA\text{-}H]^- + HCO_4$	107.5	109.3	$IAA + CO_4^- \rightarrow [IAA + O_2]^- + CO_2$	−64.3	−57.1
$IPA + CO_4^- \rightarrow [IPA\text{-}H]^- + HCO_4$	108.7	115.8	$IPA + CO_4^- \rightarrow [IPA + O_2]^- + CO_2$	−69.6	−52.0
$IBA + CO_4^- \rightarrow [IBA\text{-}H]^- + HCO_4$	109.1	117.4	$IBA + CO_4^- \rightarrow [IBA + O_2]^- + CO_2$	−66.4	−48.2
$IAA + Cl^- \rightarrow [IAA\text{-}H]^- + HCl$	41.3	30.2	$IAA + Cl^- \rightarrow [IAA + Cl]^-$	−109.7	−76.2
$IPA + Cl^- \rightarrow [IPA\text{-}H]^- + HCl$	42.6	36.7	$IPA + Cl^- \rightarrow [IPA + Cl]^-$	−112.2	−76.4
$IBA + Cl^- \rightarrow [IBA\text{-}H]^- + HCl$	42.9	38.4	$IBA + Cl^- \rightarrow [IBA + Cl]^-$	−106.7	−75.4
$IAA + Br^- \rightarrow [IAA\text{-}H]^- + HBr$	78.7	67.1	$IAA + Br^- \rightarrow [IAA + Br]^-$	−90.8	−58.5
$IPA + Br^- \rightarrow [IPA\text{-}H]^- + HBr$	79.8	73.6	$IPA + Br^- \rightarrow [IPA + Br]^-$	−92.7	−58.2
$IBA + Br^- \rightarrow [IBA\text{-}H]^- + HBr$	80.2	75.2	$IBA + Br^- \rightarrow [IBA + Br]^-$	−89.8	−59.0

$[M + O_2]^-$ from O_2^- is thermodynamically more favorable than its formation from $[CO_2 + O_2]^-$. Although deprotonation of IPA and IBA is thermodynamically possible, these compounds are weaker acids than IAA. Furthermore, IPA and IBA form more stable adduct anions with O_2^- compared to IAA. These can be the reasons why IPA and IBA have less tendency for deprotonation.

The mass spectra show that for all three auxins, the ion mobility peak at higher drift times is related to of anionic dimers $[2\ M\text{-}H]^-$. Table S2 shows that the stability trend for the anionic dimers is as $[2IBA\text{-}H]^- > [2IPA\text{-}H]^- > [2IAA\text{-}H]^-$ indicating that even if some $[IBA\text{-}H]^-$ are formed, they have tendency to form dimers and $[IBA\text{-}H]^-$ ions are depleted in the ionization region. The optimized structures of the most stable isomers of the anionic dimers of IAA, IPA, and IBA are shown in Figure S7 (Electronic Supplementary Materials). Comparison of these structures reveals that the stability trend is in accordance with the number of hydrogen bonds between COO^- group of $[M\text{-}H]^-$ ions and CH, NH, and OH groups of the neutral auxins. In the positive polarity, proton-bound dimers of auxins, $[2\ M + H]^+$, were not detected, even at high concentrations. Previous studies on the acidic compounds reported similar results for the dimer formation and attributed it to lower affinity of $[M\text{-}H]^-$ for hydration compared to $[M + H]^+$, because formation of dimers from hydrated ions is thermodynamically less favored [43].

Figures 6a and b compare ion mobility spectra of the auxins in the presence of dopant gases tetrachloride carbon and bromoform. Only one ion mobility peak is observed for each auxin. Mass spectra in Fig. 6c and d confirm that these peaks are due to halide attachment to auxins and formation of adduct ions $[M + Cl]^-$ and $[M + Br]^-$. The auxins with an acidic COOH group are expected to be ionized by deprotonation; however, calculations show that Cl^- and Br^- are weaker bases than O_2^- and cannot deprotonate auxins (Table 2). As the auxins have different hydrogen bond donor sites, different isomeric adduct ions are possible for $[M + Cl]^-$ and $[M + Br]^-$. The optimized structures of the possible isomers of adduct anions of IAA, IPA, and IBA with Cl^- and Br^- are shown in Figures S8 and S9 (Electronic Supplementary Materials), respectively. Comparison of the calculated ΔH and ΔG values in Table 2 shows that formation of both $[M + Cl]^-$ and $[M + Br]^-$ is thermodynamically favored; however, $[M + Cl]^-$ adducts are more stable compared to $[M + Br]^-$ by about 20 kJ mol^{-1} indicating stronger hydrogen bonding interactions in the former.

Separation of auxins mixture by IMS

Figure 7 shows the ion mobility spectra of a mixture of IAA, IPA, and IBA in different polarities and in the presence of NH_3, CCl_4, and $CHBr_3$ dopants. In the normal positive mode, as the ionization mechanism for all the auxins is protonation, three distinguished peaks are observed for the auxin mixture (Fig. 7a). However, in the positive polarity and in the presence of NH_3 dopant, the ionization mechanism becomes more complicated, IAA is ionized by NH_4^+ attachment (one IM-peak) while IPA and IBA are ionized by both protonation and NH_4^+ attachment (two peaks for each auxin). Hence, with NH_4^+ ionization, the peaks overlap and separation of the auxin is not possible (Fig. 7b). This indicates the importance of removal NH_3 impurity in the drift gas or in the ion source to avoid NH_4^+ attachment and overlapping of the auxin peaks when the measurements are carried

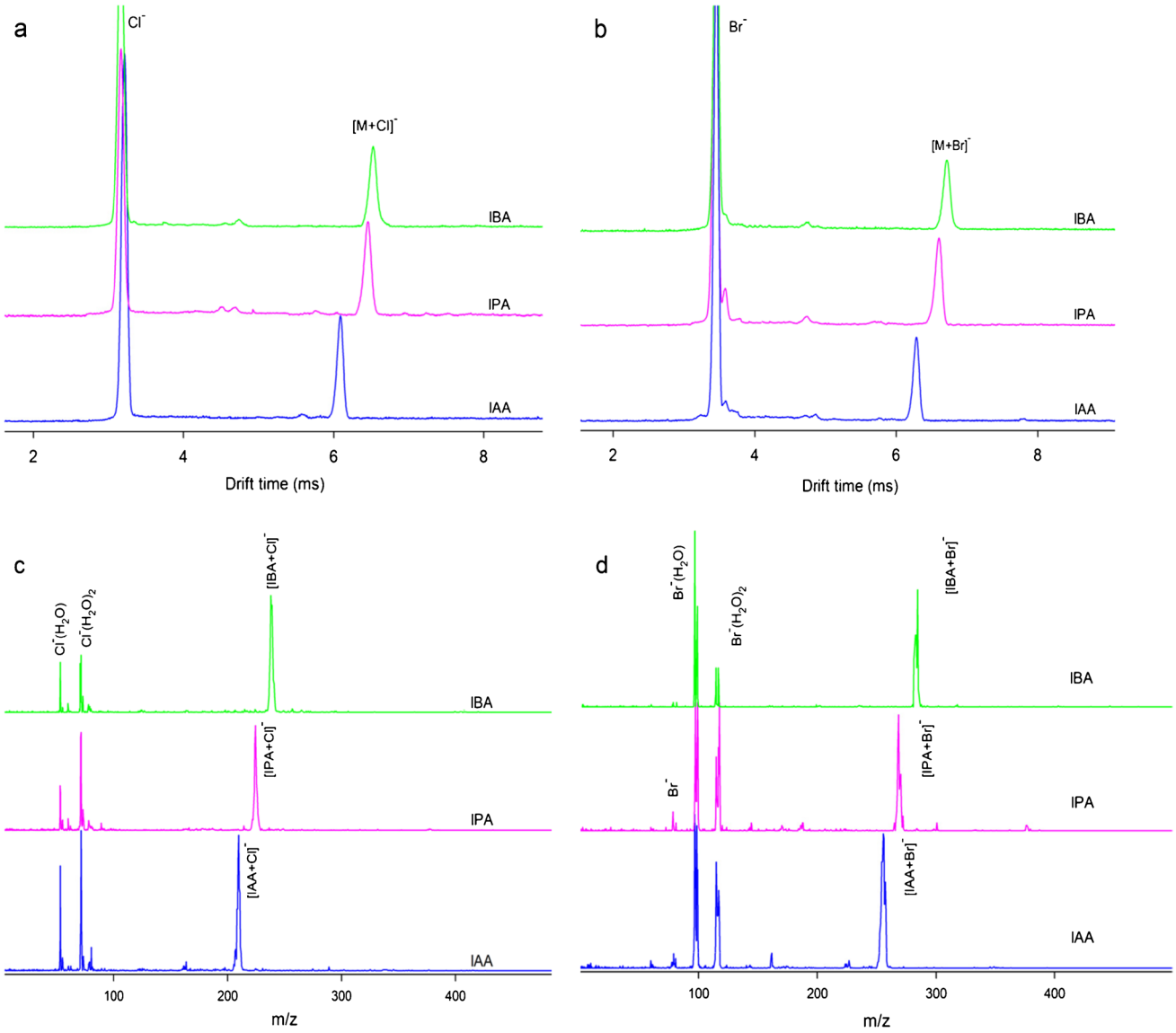

Fig. 6 Ion mobility spectra of IAA, IPA, and IBA (30 mg $L.^{-1}$) in the negative mode with **a** CCl_4 and **b** $CHBr_3$ dopants. Mass spectra with **c** CCl_4 and **d** $CHBr_3$ dopants

out in the positive polarity. In the negative polarity and absence of dopants, the peaks of monomers cannot be used for separation of the auxins. As IAA is ionized by deprotonation, $[M\text{-}H]^-$, and IPA and IBA form adduct anions with O_2^-, $[M + O_2]^-$, there is no regular drift time difference between the IM-peaks and these peaks are not appropriate for mixture analysis (Fig. 7c). However, three well-separated peaks are observed for the anionic dimers $[2\ M\text{-}H]^-$ in the mixture (Fig. 7c). In case of CCl_4 and $CHBr_3$ dopants in negative polarity, the IM-peaks of IPA and IBA are very close to each other and they overlap partially; however, more significant peak separation is observed for CCl_4 dopant. In summary, the use of the $[M + H]^+$ and $[2\ M\text{-}H]^-$ peaks in the normal positive and negative polarities, respectively, in the absence of dopants leads to more efficient separation of the auxins in the mixtures. Although in the negative polarity, due to three different ionization pathways including deprotonation, O_2^- attachment, and dimer formation, the IM-spectrum contains several peaks (Fig. 7c), more peak separation is observed compared to the positive mode. Effect of concentration of the auxins in the mixture on the peak separation was also investigated. Figure S10 (Electronic Supplementary Materials) compares that ion mobility spectra of the auxin mixture with different concentrations (15, 25, 50 mg L^{-1}) in the positive and

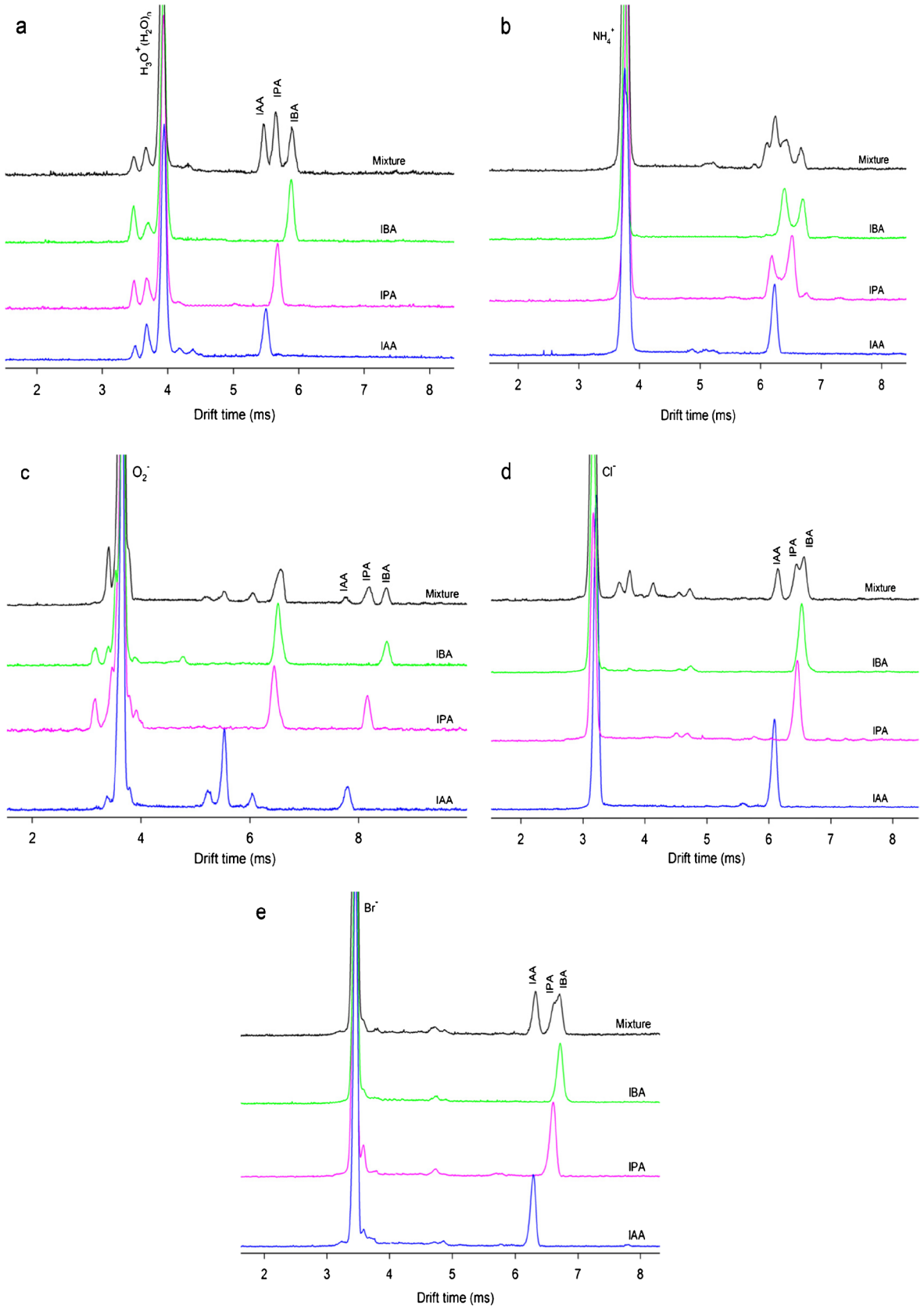

Fig. 7 Ion mobility spectra for a mixture of IAA, IPA, and IBA in **a** positive mode, **b** positive mode with NH_3 dopant, **c** negative mode, **d** negative mode with CCl_4 dopant, and **e** negative mode with $CHBr_3$ dopant. Concentrations of IAA, IPA, and IBA in the mixture are 30 mg $L.^{-1}$

negative modes of the ion source. This range of concentration does not have considerable effect on the peak separation, and only the signal intensities increase with increase in concentration.

The auxins were ionized via different reactions including protonation, ammonium attachment, deprotonation, and halide attachment. For this reason, calibration curves and the limits of detection (LODs) were determined for the auxins in all ionization conditions. For the negative mode without dopants, the dimer peaks were considered as the analytical signals to obtain calibration curves. The LODs were determined as the concentration in which the signal to noise ratio is ~ 3. The linear ranges and the LODs in different conditions are summarized in Table 3. For all the auxins, wider linear ranges are obtained with CCl_4 and $CHBr_3$ dopants. Although the obtained LODs in different conditions are similar, the negative mode without dopants shows the highest LODs for IAA and IBA. Generally, the best sensitivity and linear range for detection of the auxins by IMS is observed for the negative mode with CCl_4 dopants.

The reported LODs for auxin obtained by GC–MS are in the range of pg [44, 45] indicating the lower sensitivity of IMS compared to GC–MS. The LODs obtained by IMS are comparable with those reported for HPLC with fluorescence (FL) detector (pmol ~ ng) [46]. The amount of IAA in 1 g tobacco leaf is 1–3 ng [44]. Hence, the IMS method presented in this work can detect auxins in real plant leaves with weight of ≥ 1 g. In a previous study, HPLC-FL method with comparable LOD has been successfully used for measurement of auxins in 0.3–2 g of wheat and tobacco leaves [46]. It should be mentioned that the LODs obtained in our work are for direct injection; therefore, preconcentration or using solid phase microextraction (SPME-IMS) will further enhance the sensitivity [47]. Alternatively, derivatization of auxins is a simple method improving their LODs. To prove it experimentally, the effect of methylation (esterification) of IAA on the sensitivity of IMS was investigated (Figure S2). Interestingly, methylation of IAA decreased the LODs by about one order in the positive mode without any dopant. This can be due to (i) increase of the basicity of IAA after methylation from 850 to 878 kJ mol^{-1} and (ii) increase in the volatility of IAA improving vaporization efficiency in the injection port. Although IMS showed lower sensitivity relative to the chromatographic techniques, the measurement runtimes of IMS are in ms scale leading to faster analysis of auxins.

As the auxins are acidic compounds, they are easily ionized in the negative mode. Most of the chemical compounds in plant tissues are not ionized in the negative mode while they show intense signals in the positive mode and consequently interfere the auxin analysis. Hence, negative mode is recommended for measurement of the auxins in the real plant tissues.

Conclusion

APCI-CD-IMS-MS was used to study ionization mechanism and separation of three auxin plant hormones. Both the nature of the reactant ions in APCI-CD and the structure of the auxins influenced the ionization mechanisms. In the positive polarity, the auxins are ionized by protonation and NH_4^+ attachment, and in the negative polarity, deprotonation and anion attachment are the main ionization pathways. It was found that efficiency of IMS for separation of a mixture of the auxins depends on both ion polarity and on the dopants, which modify the RIs. In the positive polarity, the protonation of auxins, $[M+H]^+$, resulted in appearance of three distinguished IM-peaks for the mixture of auxins. In the negative polarity, the best separation was achieved for the anionic dimers $[2\ M\text{-}H]^-$. In the case of ionization resulting in formation of several product ions (more ionization pathway), the separation power of IMS decreases due to overlap of auxin peaks. For the separation of the mixtures of auxins, the optimum method is the positive polarity without NH_3 dopant. The LOD obtained in the negative mode of IMS with CCl_4 dopant is about 4 ng. Although this sensitivity is adequate for detection of auxins in the plant tissues, methylation of auxins can be used for furthermore improvement in sensitivity.

Table 3 The LODs and linear ranges (in ng) for IAA, IPA, and IBA obtained by CD-IMS in the positive and negative polarities with different dopants

	IAA		IPA		IBA	
Polarity/dopant	Linear range	LOD	Linear range	LOD	Linear range	LOD
Positive	15–60	5	10–60	4	15–60	6
Positive + NH_3	10–60	4	15–60	6	12–50	4
Negative	25–80	12	8–50	3	25–70	10
Negative + CCl_4	8–80	3	10–100	4	10–100	4
Negative + $CHBr_3$	15–60	5	15–90	5	12–100	4

Supplementary Information The online version contains supplementary material available at https://doi.org/10.1007/s00216-022-04198-x.

Funding V.I. thanks the European Union's Horizon 2020 research and innovation programme under the Marie Sklodowska-Curie grant agreement No. 101031538. This research was also partially supported by Slovak Research and Development Agency under project Nr. APVV-19–0386.

Declarations

Conflict of interest The authors declare no competing interests.

References

1. Simon S, Petrasek J. Why plants need more than one type of auxin. Plant Sci. 2011;180:454–60.
2. Ludwig-Muller J. Auxin conjugates: their role for plant development and in the evolution of land plants. J Exp Bot. 2011;62:1757–73.
3. Fendrych M, Akhmonova M, Merrin J, Glanc M, Hagihara S, Takahashi K, Uchida N, Torii KU, Firml J. Rapid and reversible root growth inhibition by TIR1 auxin signalling. Nat Plant. 2018;4:453–9.
4. Frim J. Auxin transport-shaping the plant. Curr Opin Plant Biol. 2003;6:7–12.
5. Zivanovic BD, Ullrich KK, Steffens B, Spasic SZ, Galland P. The effect of auxin (indole-3-acetic acid) on the growth rate and tropism of the sporangiophore of phycomyces blakesleeanus and identification of auxin-related genes. Protoplasma. 2018;255:1331–47.
6. Sorefan K, Girin T, Liljegren SJ, Ljung K, Robles P, Galvan-Ampudia CS, Offering R, Friml J, Yanofsky MF, Ostergaard L. A regulated auxin minimum is required for seed dispersal in Arabidopsis. Nature. 2009;459:583–6.
7. McSteen P, Malcomber S, Skirpan A, Lunde C, Wu X, Kellogg E, Hake S. Barren inflorescence2 encodes a co-ortholog of the PINOID serine/threonine kinase and is required for organogenesis during inflorescence and vegetative development in maize. Plant Physiol. 2007;144:1000–11.
8. Du F, Ruan G, Liu H. Analytical methods for tracing plant hormones. Anal Bioanal Chem. 2012;403:55–74.
9. Porfirio S, Gomes da Silva MDR, Peixe A, Cabrita MJ, Azadi P. Current analytical methods for plant auxin quantification—a review. Anal Chim Acta. 2016;902:8–21.
10. Hu Y, Li Y, Zhang Y, Li G, Chen Y. Development of sample preparation method for auxin analysis in plants by vacuum microwave-assisted extraction combined with molecularly imprinted clean-up procedure. Anal Bioanal Chem. 2011;399:3367–74.
11. Zhang R, Li S, Liu X, Zhang H. Development of a nitrogen-rich hyperbranched polymer as adsorbent for enrichment and determination of auxins in plants. Anal Bioanal Chem. 2019;411:1409–19.
12. Prinsen E, Dongen WV, Esmans EL, Onckelen HAV. HPLC linked electrospray tandem mass spectrometry: a rapid and reliable method to analyse indole-3-acetic acid metabolism in bacteria. J Mass Spectrom. 1997;32:12–22.
13. Dobrev PI, Hoyerova K, Petrasek J. Analytical determination of auxins and cytokinins. Methods Mol Biol. 2017;1569:31–9.
14. Cao ZY, Sun LH, Mou RX, Zhang LP, Lin XY, Zhu ZW, Chen MX. Profiling of phytohormones and their major metabolites in rice using binary solid-phase extraction and liquid chromatography-triple quadrupole mass spectrometry. J Chromatogr A. 2016;1451:67–74.
15. Wang L, Zou Y, Kaw HY, Wang G, Sun H, Cai L, Li C, Meng LY, Li D. Recent developments and emerging trends of mass spectrometric methods in plant hormone analysis: a review. Plant Methods. 2020;16:54.
16. Zhang H, Tan SN, Teo CH, Yew YR, Ge L, Chen X, Yong JWH. Analysis of phytohormones in vermicompost using a novel combinative sample preparation strategy of ultrasound-assisted extraction and solid-phase extraction coupled with liquid chromatography-tandem mass spectrometry. Talanta. 2015;139:89–197.
17. Novak O, Flokova K. An UHPLC-MS/MS method for target profiling of stress-related phytohormones. Methods Mol Biol. 2018;1778:183–92.
18. Cao D, Barbier F, Yoneyama K, Beveridge CA. A rapid method for quantifying RNA and phytohormones from a small amount of plant tissue. Front Plant Sci. 2020;11:605069.
19. Owen SJ, Abrams SR. Measurement of plant hormones by liquid chromatography-mass spectrometry. Methods Mol Biol. 2009;495:39–51.
20. Barkawi LS, Tam YY, Tillman JA, Normanly J, Cohen JD. A high-throughput method for the quantitative analysis of auxins. Nat Protoc. 2010;5:1609–18.
21. Barkawi LS, Tam YY, Tillman JA, Pederson B, Calio J, Al-Amier H, Emerick M, Normanly J, Cohen JD. A high-throughput method for the quantitative analysis of indole-3-acetic acid and other auxins from plant tissue. Anal Biochem. 2008;372:177–88.
22. Schummer C, Delhomme O, Appenzeller BM, Wennig R, Millet M. Comparison of MTBSTFA and BSTFA in derivatization reactions of polar compounds prior to GC/MS analysis. Talanta. 2009;77:1473–82.
23. Underberg WJM, Waterval JCM. Derivatization trends in capillary electrophoresis: an update. Electrophoresis. 2002;23:3922–33.
24. Yin XB, Guo JM, Wei W. Dual-cloud point extraction and tertiary amine labelling for selective and sensitive capillary electrophoresis-electrochemiluminescent detection of auxins. J Chromatogr A. 2010;1217:1399–406.
25. Isoda R, Yoshinar A, Ishikawa Y, Sadoine M, Simon R, Frommer WB, Nakamura M. Sensors for the quantification, localization and analysis of the dynamics of plant hormones. Plant J. 2021;105:542–57.
26. Walia A, Waadt R, Jones AM. Genetically encoded biosensors in plants: pathways to discovery. Annual Rev Plant Biol. 2018;69:497–524.
27. Waadt R. Phytohormone signaling mechanisms and genetic methods for their modulation and detection. Curr Opin Plant Biol. 2020;57:31–40.
28. Eiceman GA, Karpas Z, Hill HH. Ion mobility spectrometry. 3rd ed. Taylor & Francis Group, Boca Raton, Fl: CRC Press; 2014.
29. Marchand A, Livet S, Rosu F, Gabelica V. Drift tube ion mobility: how to reconstruct collision cross section distributions from arrival time distributions? Anal Chem. 2017;89:12674–81.
30. Sunner J, Nicol G, Kebarle P. Factors determining relative sensitivity of analytes in positive mode atmospheric pressure ionization mass spectrometry. Anal Chem. 1988;60:1300–7.
31. Ewing RG, Eiceman G, Stone JA. Proton-bound cluster ions in ion mobility spectrometry. Int J Mass Spectrom. 1999;193:57–68.
32. Makinen M, Sillanpaa M, Viitanen AK, Knap A, Makela JM, Puton J. The effect of humidity on sensitivity of amine detection in ion mobility spectrometry. Talanta. 2011;84:116–21.
33. Valadbeigi Y, Farrokhpour H, Tabrizchi M. Effect of hydration on the kinetics of proton-bound dimer formation: experimental and theoretical study. J Phys Chem A. 2014;118:7663–71.
34. Sabo M, Okuyama Y, Kucera M, Matejcik S. Transport and stability of negative ions generated by negative corona discharge

in air studied by ion mobility-oaTOF spectrometry. Int J Mass Spectrom. 2013;334:19–26.
35. Waraksa E, Perycz U, Namiesnik J, Sillanpaa M, Dymerski T, Wojtowicz M, Puton J. Dopants and gas modifiers in ion mobility spectrometry. Trend Anal Chem. 2016;82:237–49.
36. Valadbeigi Y, Ilbeigi V, Michalczuk B, Sabo M, Matejcik S. Study of atmospheric pressure chemical ionization mechanism in corona discharge ion source with and without NH_3 dopant by ion mobility spectrometry combined with mass spectrometry: a theoretical and experimental study. J Phys Chem A. 2019;123:313–22.
37. Daum KA, Atkinson DA, Ewing RG, Knighton WB, Grimsurd EP. Resolving interferences in negative mode ion mobility spectrometry using selective reactant ion chemistry. Talanta. 2001;54:299–306.
38. Valadbeigi Y, Ilbeigi V. Using gas-phase chloride attachment for selective detection of morphine in a morphine/codeine mixture by ion mobility spectrometry. Rapid Commun Mass Spectrom. 2021;35:e9044.
39. Sabo M, Matejcik S. Corona discharge ion mobility spectrometry with orthogonal acceleration time of flight mass spectrometry for monitoring of volatile organic compounds. Anal Chem. 2012;84:5327–34.
40. Weston TR, Derner JD, Murrieta CM, Rule DC, Hess BW. Comparison of catalysts for direct transesterification of fatty acids in freeze-dried forage samples. Crop Sci. 2008;48:1636–41.
41. Frisch MJ, Trucks GW, Schlegel HB, Scuseria GE, Robb MA, Cheeseman JR, Scalmani G, Barone V, Mennucci B, Petersson GA, et al. Gaussian 09, Revision A.1; Gaussian, Inc.: Wallingford, CT, 2009.
42. Hunter EPL, Lias SG. Evaluated gas phase basicities and proton affinities of molecules: an update. J Phys Chem Ref Data. 1998;27:413–656.
43. Valadbeigi Y, Azizmohammadi S, Ilbeigi V. Small host–guest systems in the gas phase: tartaric acid as a host for both anionic and cationic guests in the atmospheric pressure chemical ionization source of ion mobility spectrometry. J Phys Chem A. 2020;124:3386–97.
44. Edlund A, Eklof S, Sundberg B, Mortiz T, Sandber G. A microscale technique for gas chromatography-mass spectrometry measurements of picogram amounts of indole-3-acetic acid in plant tissues. Plant Physol. 1995;108:1043–7.
45. Muller A, Duchting P, Weiler EW. A multiplex GC-MS/MS technique for the sensitive and quantitative single-run analysis of acidic phytohormones and related compounds, and its application to Arabidopsis thaliana. Planta. 2002;216:44–56.
46. Dobrev PI, Havlicek L, Vanger M, Malbeck J, Kaminek M. Purification and determination of plant hormones auxin and abscisic acid using solid phase extraction and two-dimensional high performance liquid chromatography. J Chromatogr A. 2005;1075:159–66.
47. Alizadeh N, Mohammadi A, Tabrizchi M. Rapid screening of methamphetamines in human serum by headspace solid-phase microextraction using a dodecylsulfate-doped polypyrrole film coupled to ion mobility spectrometry. J Chromatogr A. 2008;1183:21–8.